Available online at www.sciencedirect.com

ScienceDirect

Procedia Structural Integrity 8 (2018) 154–162

Structural Integrity Procedia

www.elsevier.com/locate/procedia

AIAS 2017 International Conference on Stress Analysis, AIAS 2017, 6-9 September 2017, Pisa, Italy

Defect Detection in Additively Manufactured Components: Laser Ultrasound and Laser Thermography Comparison

Donatella Cerniglia[a]*, Nicola Montinaro[a]

[a]*Dipartimento dell'Innovazione Industriale e Digitale, Università degli Studi di Palermo, viale delle scienze Ed. 8, 90128 Palermo, Italy*

Abstract

Despite continuous technological advances in additive manufacturing, the lack of non-destructive inspection techniques during the manufacturing process is a limit for the industrial breakthroughs. Additive manufacturing is mainly used in industrial sectors where the zero defect target is crucial. The inclusion of the integrity assessment into the additive manufacturing process would allow corrective actions to be performed before the component is completed. To this end, the development of in-process monitoring and processing techniques is of great interest.
This work proposes and compares two remote non-destructive inspection techniques: laser ultrasound and laser thermography. The two techniques are evaluated on Inconel samples with laser drilling holes to establish their sensitivity. Experimental results show that those discontinuities are efficiently detected with both techniques. The remote inspection by optical methods would allow the integration of the evaluation system into the additive manufacturing equipment, thus allowing continuous monitoring throughout the entire production process. Potential benefits and limitations of the two techniques are discussed.

Peer-review under responsibility of the Scientific Committee of AIAS 2017 International Conference on Stress Analysis

Keywords: Additive Manufacturing; IR Thermography; Laser Ultrasound; Defect Sensitivity

1. Introduction

In the last decade, additive manufacturing (AM) process has gained an increasing attention for the production of 3D geometries or repair of high-value components. Very fine and complex structures can be built up layer upon

* Corresponding author. Tel.: +39 091 23897258
E-mail address: donatella.cerniglia@unipa.it

2452-3216
Peer-review under responsibility of the Scientific Committee of AIAS 2017 International Conference on Stress Analysis
10.1016/j.prostr.2017.12.016

layer. Better accuracy for complex structures can be achieved with AM if compared to traditional manufacturing methods. Moreover, mechanical properties of AM components approach and in some cases exceed the properties found in conventionally processed structures, as shown in Lewis et al. (2000). Interlayer and intralayer defects are often observed in AM components as shown by Ahsan et al. (2011) using scanning electron microscopy and microcomputed tomography.

Additive manufacturing seems to be a potentially growing market in every manufacturing sector such as automotive, aerospace, military and medical. New and improved technologies, large application area and ease of development of custom products are the major drivers that can push the AM market. However, a few factors restraining the growth of this market are material characterization during development, process control and integrity control. In-line inspection has important implications for those sectors where validation of AM components has until now been difficult to achieve. Conventional non-destructive techniques (NDT) cannot cope with the complicated geometries typically produced by additive manufacturing. Currently, the quality of AM components is assessed by destructive testing or by X-ray computed tomography (CT) (Thompson et al. (2016)) after the part is finished, which means that parts may be rejected after all the manufacturing is completed.

For critical requirements of quality, even in parts with complex forms, the desired solution is a non-destructive technique that allows in-line inspection and detection of flaws as the layer is deposited, so that the process can be controlled and corrected. Moreover, the non-destructive technique should detect micrometric flaws that are typical in AM products.

Some NDTs for AM parts have been investigated. The use of an ultrasonic squirter probe with a standard industrial robot to inspect a 3D metal deposition structure is demonstrated by Nilsson et al. (2012). Laser-generated surface waves have been used by Nemeth et al. (2005) to interrogate laser powder deposition parts, in both stainless steel and titanium, with pores that are simulated using blind holes. Clark et al. (2011) have shown the potential of an all-optical scanning acoustic microscope instrument for online inspection of AM products.

The use of ultrasonic laser transmitter and receiver and the interaction of the incident wave with sub-surface and surface defects have been widely investigated for many different applications (Kromine et al. (2000), Klein et al. (2004), Edwards et al. (2011), Pelivanov et al. (2014), Cerniglia et al. (2015)).

A promising NDT active thermographic technique, recently used for the surface crack sizing with micrometric aperture, is the flying laser spot technique. Li et al. (2011) developed a thermographic imaging technique using the second spatial derivative of acquired flying laser spot and line thermograms, in order to characterise micrometers cracks in metal samples. Burrows et al. (2007) used the laser spot imaging thermography and, simultaneously, laser-based ultrasonic measurements to find surface breaking cracks. Using the same flying laser spot set-up with a novel post-processing approach, Montinaro et al. (2017) have successfully implemented the technique for the detection and characterisations of disbond and delamination in fibre metal laminates. The thermal footprint left by the moving heat source is monitored, looking for thermal anomalies in a region of interest via a statistical approach.

The aim of this work is to prove and compare the laser ultrasound and laser thermography as techniques that might be deployed for the inspection of AM layers to detect near-surface and surface defects. The two NDT techniques have been tested and evaluated on Inconel samples with micrometric laser drilling holes. Potential benefits and limitations of the two inspection techniques are discussed.

2. Experimental procedure

2.1. Samples

Reference samples in Inconel 600 have been used. Flaws were created in standard geometries to establish the sensitivity to defect detection. Laser drilling was used to create holes in the samples, with different diameters (ϕ) and depths (d) below the surface. The two geometries of samples are shown in Fig. 1. Sample 1 is a plate with holes below faces A and B at different distances from the edge (Fig. 1(a)); sample 2 has a raised portion, representing the first layer above the substrate, where holes were drilled (Fig. 1(b)). After laser drilling, dimensions and depths of the holes were measured. Flaw sizes and depths are reported in Table 1.

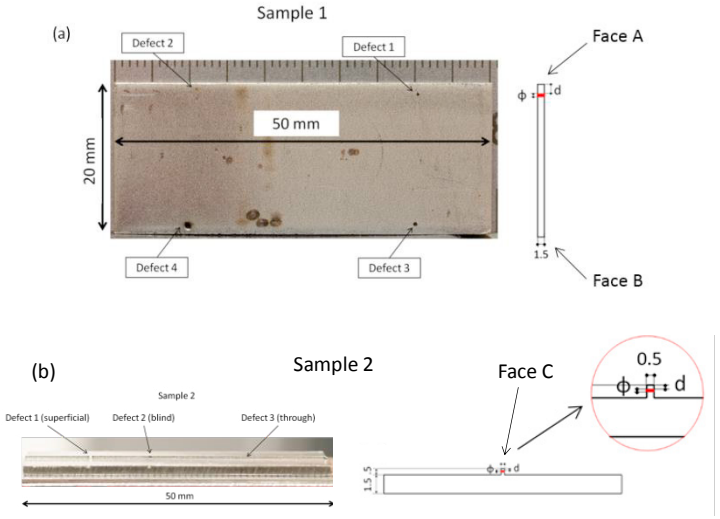

Fig. 1. The two geometries of Inconel samples: sample 1 with 4 through holes (a) and sample 2 with 3 holes, among which one superficial and one blind (b).

Table 1. Dimensions and depths of laser drilling holes.

Defect/sample	ϕ Diameter back/front side (Mean) [μm]	d Depth [mm]
1/1	700/250 (470)	1.3
2/1	660/190 (420)	0.6
3/1	800/490 (640)	0.88
4/1	440/850 (640)	0.9
1/2	(490)	0
2/2	blind/360	0.1
3/2	70/330 (200)	0.3

2.2. Laser ultrasound

The ultrasonic inspection system consists of an infrared Nd:YAG pulsed laser, used as source of acoustic waves, and a laser receiver, which combines a continuous-wave (CW) laser and an interferometric unit, to acquire the surface displacement. Wideband ultrasonic waves are generated with nanosecond laser pulses. The laser receiver produces a time-varying analog signal that is proportional to the instantaneous surface displacement. The output signals from the laser receiver are digitized by an analog-to-digital board converter, triggered by the pulsed laser, and transferred to a PC for further signal processing. Fig. 2(a) shows the experimental set-up and Table 2 the specifications of the system.

The two laser beams are directed to the sample surface by means of mirrors (for the laser transmitter) and the optical head (for the laser receiver). The two lasers are connected to the controller station (see Fig. 2(b)) with optical fibers and cables. The laser beam source is focused by two cylindrical lenses, with perpendicular axes, into a 0.1 mm x 0.3 mm line. Source-to-receiver distance is 1 mm.

The inspection of the sample is done by acquiring the ultrasonic signals and the relative coordinates along a line, with acquisitions at 0.1 mm steps. Fig. 3 shows the typical A-scan signal; the direct longitudinal (L) wave, that travels from source to receiver just below the surface, at 12 MHz and the surface (S) wave at 4 MHz are indicated. Their disruption indicates a surface and sub-surface breaking flaws. The time window was selected to monitor the surface wave (S) for sub-surface and surface defects, and, in case, the reflection of bulk longitudinal waves (R)

indicating inner discontinuities. The inspection procedure consists of acquiring the A-scans along a line on the sample surface, and showing the B-scan image (amplitude - time of flight - length of inspection). The analysis of the B-scan image allows an accurate evaluation of location, size and depth of the flaw as shown in Scafidi et al. (2015).

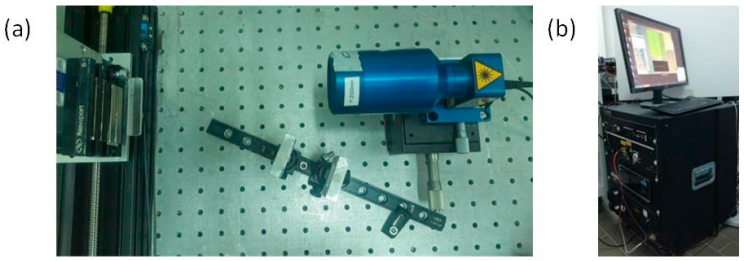

Fig. 2. Set-up for the laser ultrasound experiments (a) and the laser controller station (b).

Table 2. Specifications of the laser ultrasound system.

Laser transmitter			Laser receiver
Energy	100 mJ	Power	1 W
Wavelength	1064 nm	Wavelength	532 nm
Pulse duration	8.5 nsec	Detection bandwidth	1 MHz – 50 MHz
Frequency	20 Hz	Optical stand-off	200 mm
Beam diameter	4 mm	Laser spot	200 μm
		Diameter of collecting aperture	50 mm

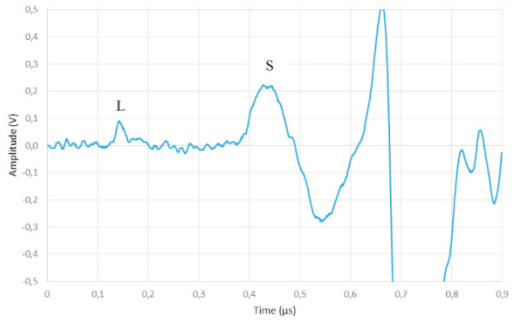

Fig. 3. A-scan signal showing the longitudinal (L) and the surface (S) waves.

2.3. Laser thermography

Figure 4 shows the set-up used for the laser thermography experiments; Table 3 indicates the parameters of the set-up. The sample is mounted on a motorized linear micro-slide controlled by PC. The CW laser beam (see specifications in Table 2) is focused into a 0.75 mm spot on faces A and B of sample 1 and into a 14 mm x 0.5 mm line on face C of sample 2. The IR camera (see specifications in Table 3) is placed perpendicularly to the sample in order to reduce geometric distortions.

The evolution of the generated thermal footprint, while moving the sample at constant speed, is full-field acquired with the IR camera but monitored and evaluated only in a region of interest (ROI) by the software FLIR Research IR v. 3.4. The ROI is placed in the zone with high temperature gradients behind the heat source, at a certain distance from it (see Fig. 5). If the sample is uniform and sound, the thermal field remains unmodified under steady state conditions (i.e. constant speed). When the heat source crosses an area over a defect, the surface temperature field is disturbed, due to the temporary barrier of the heat flux perpendicularly to the scan direction. The

defect signature is found in the evolution of the Standard Deviation (SD) of the temperature distribution over the ROI.

Two different sizes of the rectangular ROI have been used in order to better fit the geometry of the two samples (Fig. 5). For sample 1 the ROI is 1.3 x 4.2 mm^2, positioned at 1.5 mm from the center of the laser spot, on the 1.5 mm side (faces A and B); for sample 2 the ROI is 0.4 x 5 mm^2, positioned at 1 mm from the center of the focused line, on the 0.5 mm side (face C).

The thermal properties of the Inconel 600 are: specific heat 444 J/kg K and thermal conductivity 14.8 W/m K. The scanning surfaces have been matt black painted to enhance and uniform the absorption/emissivity of radiant energy.

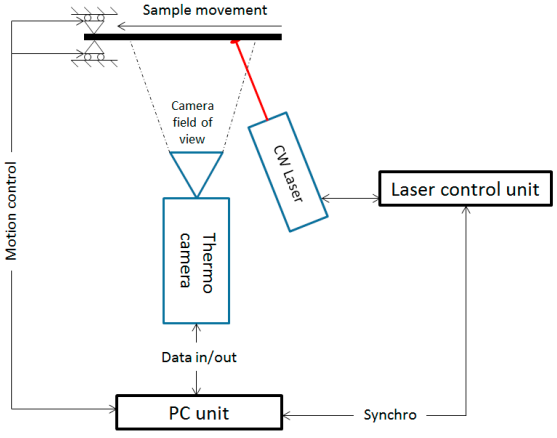

Fig. 4. Set-up for the laser thermography experiments.

Table 3. Parameters of the laser thermography set-up and specifications of the IR camera.

Set-up parameter	Value		Thermocamera
Sample/IR camera distance	~ 300 mm	Model	FLIR – X6540SC
Laser/sample surface distance	~ 300 mm	Sensor	Focal plane array
Linear micro-slide speed	5-10 mm/s	Resolution (HxV)	640 x 512 pixels
		Lens	MW 25 mm 2.0 640 x 51
		Noise (NETD)	20 mK
		Sample rate	20 Hz

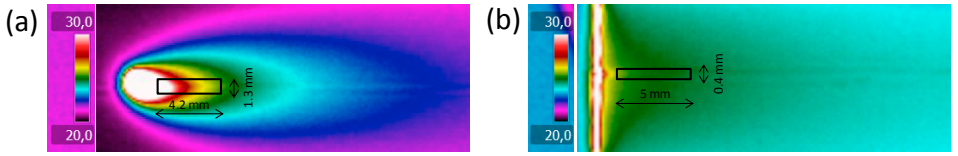

Fig. 5. Thermograms acquired on sample 1 with laser spot (a) and on sample 2 with laser line (b) with dimensions of the region of interest.

3. Experimental results

B-scan images of sample 1 are shown in Fig. 6. The ultrasonic waves at ~ 0.14 μs and at ~ 0.4 μs are the direct longitudinal wave (L) and the surface wave (S), respectively. The inner discontinuities cause reflection of the longitudinal wave propagating in the bulk. The effect is seen in the B-scan images of sample 1 on face A (Fig. 6(a)) indicating defects 1 and 2, and on face B (Fig. 6(b)) indicating defects 3 and 4.

Fig. 7 shows the typical defect signature obtained with the laser thermography, occurring when the laser flies over a defected zone. As discussed by Montinaro et al. (2017) in previous works, the detection mechanism in the flying laser inner probe technique (FLIPT) is based on the perturbation of the heat conduction perpendicularly to the scan direction. In particular, when the heat source passes over a defected zone the heat propagation is hampered causing on the sample surface a temperature raise, monitored by the IR-Camera in the ROI. After the defected zone end, the temperature decreases until its original trend. Figures 8(a) and 8(b) show the plot of SD values computed over the ROI versus the ROI position along face A and face B, respectively, on sample 1. As shown in Figs. 8, the four defects of sample 1 are correctly identified. In this case, the FLIPT technique is only able to detect the position of the defect but not its extension, that is overestimated, because of the not comparable dimensions of flaw and ROI. Experimental results obtained with laser ultrasound and laser thermography are in good agreement.

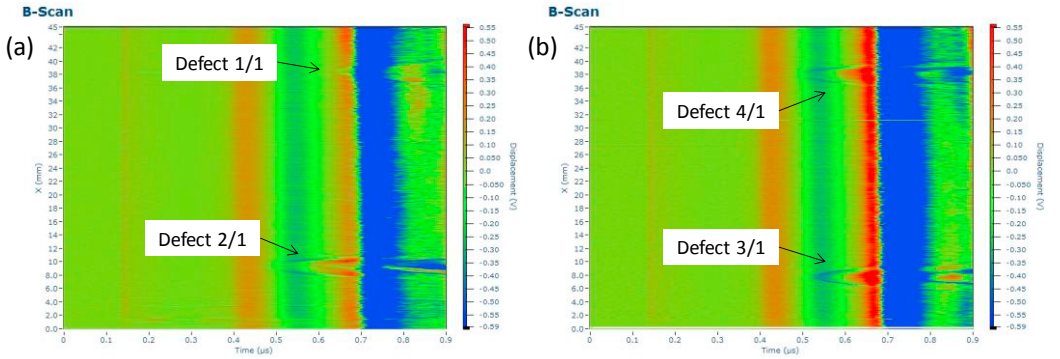

Fig. 6. B-scan images of sample 1 on face A indicating defects 1 (ϕ=470 µm, d=1.3 mm) and 2 (ϕ =420 µm, d=0.6 mm) (a), on face B indicating defects 3 (ϕ =640 µm, d=0.88 mm) and 4 (ϕ =640 µm, d=0.9 mm) (b).

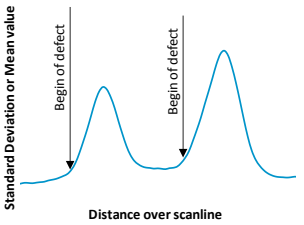

Fig. 7. Example of the perturbation on the Standard Deviation values in the ROI when approaching a defect along the scanline.

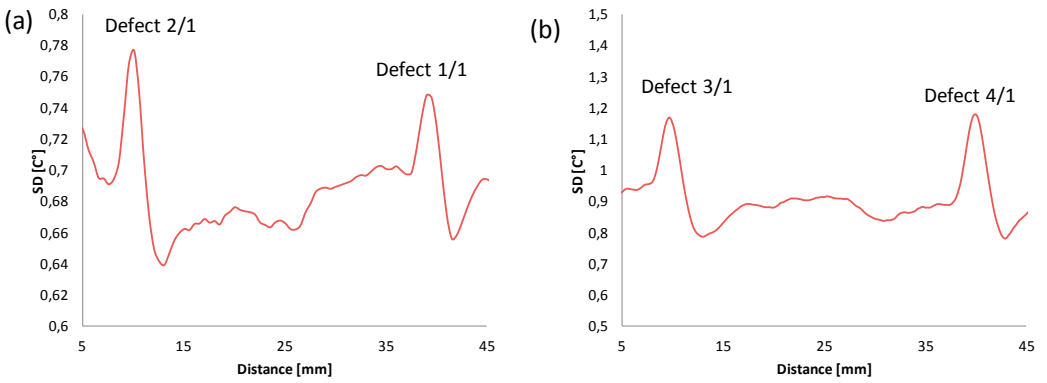

Fig. 8. Plots of SD values computed over the ROI versus the ROI position along face A (a) and face B (b) on sample 1.

B-scan image of sample 2 on face C is shown in Fig. 9(a). The disruption of the direct longitudinal (L) and the surface (S) waves at about 32 mm indicates a surface breaking defect (i.e. defect 1). The two inner discontinuities cause reflection of the longitudinal wave propagating in the bulk. The effect is seen in the B-scan image, indicating defects 2 and 3. Fig. 10 shows the A-scans relative to a flawless zone and to defect 3 that is indicated by the reflection of the longitudinal wave (R).

Fig. 9(b) shows the plot of SD values computed over the ROI versus the ROI position along face C. The perturbations on the SD value along the scanline over the sample 2 allow to spot the three defects.
Results obtained with laser ultrasound and laser thermography are in good agreement.

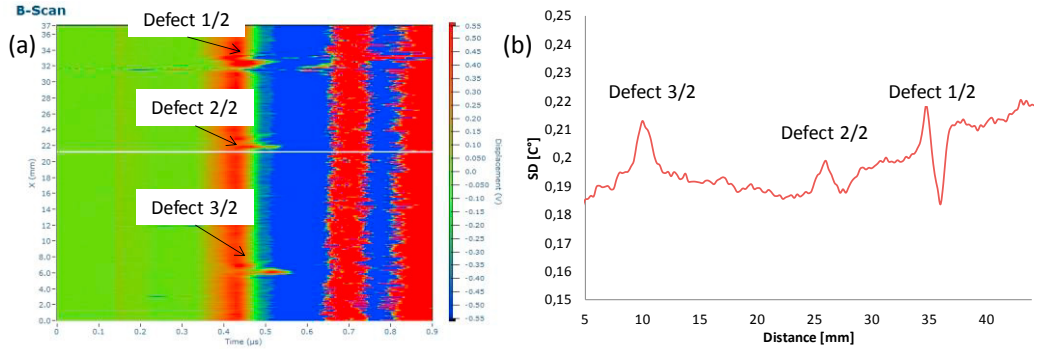

Fig. 9. (a) B-scan image of sample 2 showing defects 1 (ϕ = 490 µm, d=0 mm), 2 (ϕ = 360 µm, d=0.1 mm), 3 (ϕ =200 µm, d=0.3 mm) and (b) plot of SD value computed over the ROI versus the ROI position along face C on the sample 2.

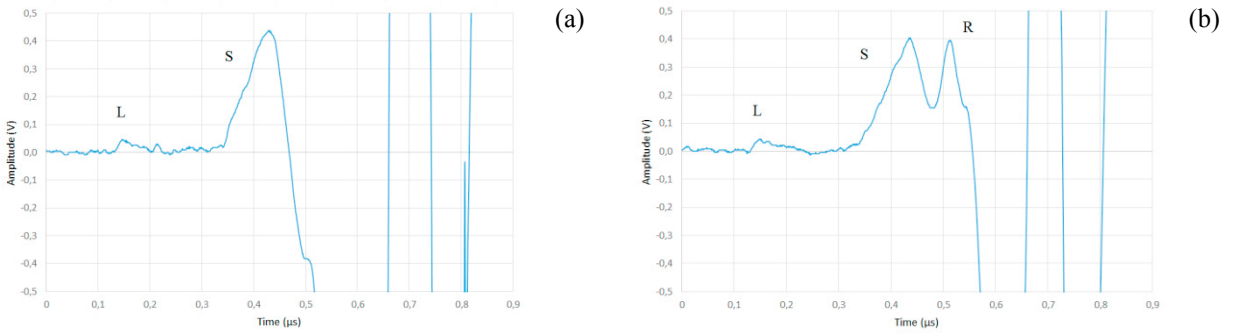

Fig. 10. A-scans relative to a flawless zone (a) and to defect 3 (ϕ =200 µm, d=0.3 mm) (b) in sample 2.

The two techniques have proved to be able to detect the typical micrometric defects of the AM products.
Laser generation has the advantage to generate simultaneously longitudinal, shear and surface waves. The radiation pattern of the longitudinal wave in the thermoelastic regime shows the highest amplitude at 50 – 70 degrees from the perpendicular axis to the surface (Scruby et al. (1990)). This feature allows to detect strong longitudinal waves reflected from a defect, at a depth greater than the thickness of a single AM layer, with the laser set-up used in this work. The laser receiver has a number of features, such as wide detection bandwidth up to 50 MHz, high sensitivity, robustness and stability. The two focused laser beams can be easily directed on small size and/or curved surfaces, otherwise difficult to access with other probes. The analysis of the B-scan image allows an accurate evaluation of location, size and depth of the flaw.

The technical benefits must be weighed along with the limitations. The laser ultrasound technique is limited for a range of flaw size/depth combination, as shown in Cerniglia et al. (2015). There are safety hazards with high-power pulsed lasers, used for the generation of ultrasonic waves, which require beam enclosures or the use of safety goggles. Inspection speed higher than 5 mm/s would increase nonlinearly the cost of the laser source. Signal-to-

noise ratio depends strongly on the light collected by the laser receiver and rough surfaces can reduce it. Moreover, the current cost of the laser ultrasound equipment is high if compared with the laser thermography set-up.

The laser thermography technique has the advantage to be very robust and easy to set. Since thermal contrast and framerate required for this particular inspection are not elevated, the use of a microbolometric IR camera, instead of a liquid cooled one, could reduce cost and overall dimension of the equipment, in order to better fit it in an automatic in-line process.

A drawback of this technique is the need to paint the scanning surface to enhance, if not sufficient, the absorption/emissivity of radiant energy. To overcome this issue a more powerful laser heat source, compatible with the material tested, could be used. Moreover, the post-processing of the technique provides an approximated evaluation of flaw location without any indication on size and depth, due to greater size of the ROI than the flaw size. This limit could be addressed.

Both techniques allow a non-contact and remote inspection. Both have potential for in-line inspection and processing, although do not allow full-field inspection but laser scanning is required.

4. Conclusion

Additive manufacturing allows to create 3D complex geometries whose inspection is a big challenge for non-destructive testing methods. Currently, the quality of AM components is assessed by destructive testing or by X-ray computed tomography after all manufacturing is completed.

The effectiveness of the laser ultrasound and laser thermography techniques to detect micrometric defects in AM components has been tested on reference samples with laser drilling holes. Defect detection is comparable among the two approaches. Benefits and limitations are highlighted for both techniques. The greater benefit is, for the laser ultrasound, the detection and evaluation of flaws, whilst, for the laser thermography, the robustness and the easy set-up. The most disadvantageous limitation is the cost for the laser ultrasound and the need of matt surfaces for the laser thermography.

The remote inspection system by optical methods could potentially be linked to the additive manufacturing rig, in order to achieve monitoring of the entire additive process. The inspection should be performed after layer deposition, when the part has reached the room temperature since the equipment cannot stand at the heat generated by the process.

Both techniques allow a non-contact and remote inspection, both having a potential for in-line automated inspection and processing. Further work is needed before this could become an alternative to existing method.

References

Ahsan, M. N., Bradley, R., Pinkerton, A. J., 2011. Microcomputed Tomography Analysis of Intralayer Porosity Generation in Laser Direct Metal Deposition and its Causes. J. Laser Appl. 23, 022009.

Burrows, S. E., Rashed, A., Almond, D.P., Dixon, S., 2007. Combined laser spot imaging thermography and ultrasonic measurements for crack detection. Nondestructive Testing and Evaluation 22, 217-227.

Cerniglia, D., Scafidi, M., Pantano, A., Rudlin, J., 2015. Inspection of additive-manufactured layered components. Ultrasonics 62, 292-298.

Clark, D., Sharples, S. D., Wright, D. C., 2011. Development of Online Inspection for Additive Manufacturing Products. Insight 53(11), 610-614.

Edwards, R. S., Dutton, B., Clough, A. R., Rosli, M. H., 2011. Scanning Laser Source and Scanning Laser Detection Techniques for Different Surface Crack Geometries. In: Review of Progress in Quantitative Nondestructive Evaluation, Proc. AIP Conference, Burlington, VT, 251-258.

Klein, M., Sears, J., 2004. Laser ultrasonic inspection of laser cladded 316LSS and Ti 6-4. Proc. 23rd Int. Congress on Applications of Lasers and Electro-Optics, San Francisco, CA.

Kromine, A. K., Fomitchov, P. A., Krishnaswamy, S., Achenbach, J. D., 2000. Laser Ultrasonic Detection of Surface Breaking Discontinuities: Scanning Laser Source Technique. Mater. Evaluation 58 (2), 173-177.

Lewis, G. K., Schlienger, E., 2000. Practical considerations and capabilities for laser assisted direct metal deposition. Mater. Des. 21, 417-423.

Li, T., Almond, D. P., Rees, D. A. S., 2011. Crack imaging by scanning laser-line thermography and laser-spot thermography. Measurement Science and Technology 22(3), 035701.

Montinaro, N., Cerniglia, D., Pitarresi, G., 2017. Detection and characterization of disbonds on fibre metal laminate hybrid composites by flying laser spot thermography. Composites Part B: Engineering 108, 164-173.

Montinaro, N., Cerniglia, D., Pitarresi, G., 2017. Flying laser spot thermography technique for the NDE of fibre metal laminates disbonds. Composite Structures 171, 63-76.

Montinaro, N., Cerniglia, D., Pitarresi, G., 2017. Flying laser spot thermography for the inspection of aerospace grade Fibre Metal Laminates. Proc. 4th IEEE Int. Workshop on Metrology for Aerospace, Padua, Italy.

Nemeth, J., Klien, M., Sears, J. W., 2005. Development of Laser Ultrasonics for Defect Detection during Laser Powder Deposition. Proc. TMS Annual Meeting & Exhibition, San Francisco, CA.

Nilsson, P., Appelgren, A., Henrikson, P., Runnemalm, A., 2012. Automatic ultrasonic testing for metal deposition. Proc. 18th World Conference on Nondestructive Testing, Durban, South Africa.

Pelivanov, I., Buma, T., Xia, J., Wei, C., O'Donnel, M., 2014. A New Fiber-Optic Non-Contact Compact Laser-Ultrasound Scanner for Fast Non-Destructive Testing and Evaluation of Aircraft Composites. J. Appl. Phys. 115, 113105.

Scafidi, M., Cerniglia, D., Ingrassia, T., 2015. 2D size, position and shape definition of defects by B-scan image analysis. Frattura ed Integrità Strutturale 9, 622-629.

Scruby C. B., Drain, L. E., 1990. Laser Ultrasonics: Techniques and applications. Adam Hilger, New York, pp. 263.

Thompson, A., Maskery, I., Leach, R. K., 2016. X-ray computed tomography for additive manufacturing: a review. Meas. Sci. Technol. 27, 072001.